



OPEN

Diffraction Interference Induced Superfocusing in Nonlinear Talbot Effect

SUBJECT AREAS:

NONLINEAR OPTICS
SUB-WAVELENGTH OPTICSDongmei Liu¹, Yong Zhang¹, Jianming Wen², Zhenhua Chen¹, Dunzhao Wei¹, Xiaopeng Hu¹, Gang Zhao¹, S. N. Zhu¹ & Min Xiao^{1,3}Received
12 May 2014Accepted
24 July 2014Published
20 August 2014

Correspondence and requests for materials should be addressed to Y.Z. (zhangyong@nju.edu.cn); J.W. (jianming.wen@yale.edu) or M.X. (mxiao@uark.edu)

¹National Laboratory of Solid State Microstructures, College of Engineering and Applied Sciences, School of Physics, Nanjing University, Nanjing 210093, China, ²Department of Applied Physics, Yale University, New Haven, Connecticut 06511, USA, ³Department of Physics, University of Arkansas, Fayetteville, Arkansas 72701, USA.

We report a simple, novel subdiffraction method, i.e. diffraction interference induced superfocusing in second-harmonic (SH) Talbot effect, to achieve focusing size of less than $\lambda_{\text{SH}}/4$ (or $\lambda_{\text{pump}}/8$) without involving evanescent waves or subwavelength apertures. By tailoring point spread functions with Fresnel diffraction interference, we observe periodic SH subdiffracted spots over a hundred of micrometers away from the sample. Our demonstration is the first experimental realization of the Toraldo di Francia's proposal pioneered 62 years ago for superresolution imaging.

Focusing of a light beam into an extremely small spot with a high energy density plays an important role in key technologies for miniaturized structures, such as lithography, optical data storage, laser material nanoprocessing and nanophotonics in confocal microscopy and superresolution imaging. Because of the wave nature of light, however, Abbe¹ discovered at the end of 19th century that diffraction prohibits the visualization of features smaller than half of the wavelength of light (also known as the Rayleigh diffraction limit) with optical instruments. Since then, many efforts have been made to improve the resolving power of optical imaging systems, and the research on overcoming the Abbe-Rayleigh diffraction limit has become an energetic topic (for recent reviews see Refs. 2–4).

Historically, an early attempt to combat the diffraction limit can be traced back to the work by Ossen⁵ in 1922, in which he proved that a substantial fraction of emitted electromagnetic energy can be squeezed into an arbitrarily small solid angle. Inspired by the concept of super-directivity⁶, in his seminal 1952 paper Toraldo di Francia⁷ suggested that a pupil design provide an accurately tailored subdiffracted spot by using a series of concentric apertures with different phases. Based on the mathematical prediction that band-limited functions are capable of oscillating faster than the highest Fourier components carried by them (a phenomenon now known as superoscillation⁸), Berry and Popescu⁹ in their recent theoretical analysis pointed out that subwavelength localizations of light could be obtained in Talbot self-imaging^{10,11} under certain conditions. With use of a nanohole array, Zheludev's group demonstrated the possibility to focus the light below the diffraction limit^{12,13}. By using a sequence of metal concentric rings with subwavelength separations, they further reported well-defined, sparsely distributed subdiffracted light localizations in a recent optical superoscillating experiment¹⁴. Despite the newly developments of quantum imaging¹⁵ and quantum lithography¹⁶ allow the formation of sub-Rayleigh diffracted spots, the severe reliance on specific quantum entangled states and sophisticated measurement devices limits their practical applications.

By exploring evanescent components containing fine details of an electromagnetic field distribution, researchers working in near-field optics have invented powerful concepts, such as total internal reflectance microscopy¹⁷ and metamaterial-based superlens^{18,19}, to overcome the barrier of the diffraction limit. Most near-field techniques operate at a distance extremely close (typically hundreds of nanometers) to the object in order to obtain substantial subdiffracted spots. Since these techniques cannot image an object beyond one wavelength, they are not applicable to image into objects thicker than one wavelength, which greatly limits their applicability in many situations. There also exists a broad category of *functional* super-resolution imaging techniques which use clever experimental tools and known limitations on the matter being imaged to reconstruct the super-resolution images. The representative ones include stimulated emission depletion²⁰, spatially-structured illumination microscopy²¹, stochastic optical reconstruction microscopy²², and super-resolution optical fluctuation imaging²³.

Principle and experimental scheme. Here we introduce an alternative scheme, i.e. diffraction interference induced superfocusing in nonlinear Talbot effect^{24,25}, to achieve subdiffraction by exploiting the phases of the



second-harmonic (SH)^{24–27} fields generated from a periodically-poled LiTaO₃ (PPLT) crystal. The poling inversions in the PPLT crystal, typically with a period of few micrometers, make the SH waves generated in the negative domains possess a π phase shift relative to those in the positive domains. The destructive interference between these two SH waves in the Fresnel diffraction region shrinks the point spread functions below the diffraction limit and leads to subwavelength focused spots, resembling a similar idea as suggested by Toraldo di Francia sixty-two years ago⁷. The essential physics behind this experiment is schematically illustrated in Fig. 1. From college textbook Optics, we know that as a circular aperture with a diameter of d (Fig. 1a) is uniformly illuminated, the focused light intensity has a spatial profile of the Airy disk with a radius of $\lambda/2d$, first noticed by Abbe as the spatial resolution limit. To beat this limit, in 1952 Toraldo di Francia theoretically discovered that if the object consists of a series of concentric apertures with different transmission amplitudes and/or phases, for example, a circular aperture with α phase and its neighboring ring with β phase (Fig. 1b), due to diffraction interference the Airy disk can be shrunk below the Abbe limit with the cost of pushing the energy into the fringe wings (see Fig. 1d). In our experiments, the “object” is the generated SH waves with a periodic binary phase distribution ($\alpha = 0$ and $\beta = \pi$) from a PPLT crystal (Fig. 1c), which is designed to produce periodic superfocused spots. To the best of our knowledge, our observation of superfocusing in nonlinear Talbot self-imaging is the first realization of Toraldo di Francia’s proposal.

Besides, because of the phase matching the generated SH signals are automatically band-limited, a key ingredient for superoscillations⁹. These two unique and coexisting features distinguish the current scheme from previous works that involve either evanescent waves, metal nanostructures, luminescent objects or quantum states. Our demonstration can be considered as the first experimental realization of the Toraldo di Francia’s proposal for subdiffraction⁷ and superresolution with superoscillations⁹ in nonlinear optics. This method allows to produce subdiffracted SH spots over 100 μm easily, and has, in principle, no fundamental lower bound to limit the focusing ability. As such, we have observed superfocused SH spots with the size of less than one quarter of the SH wavelength ($\lambda_{\text{SH}}/4$) at

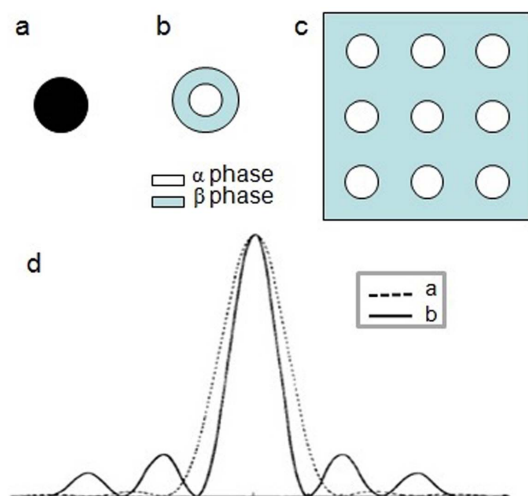


Figure 1 | Theoretical model. (a) A circular aperture. (b) A donut-like aperture with an α -phase inside circle and a β -phase outside ring. (c) The “object” in nonlinear Talbot effect, i.e., the generated SH waves with binary phases ($\alpha = 0$ and $\beta = \pi$) at the output surface of a squarely poled LiTaO₃ crystal. (d) Diffracted intensity distributions with apertures of (a) and (b) in the Fresnel near field. Obviously, the aperture (b) gives a smaller Airy disk than the aperture (a). With use of the aperture (c), periodic superfocused spots are expected to be observed in the Fresnel near field.

the distance of tens of micrometers away, which is comparable to the superoscillation experiment¹⁴, but without employing subwavelength metal nanoholes. We thus expect our imaging technique to provide a super-resolution alternative for various applications in photolithography, medical imaging, molecular imaging, as well as bioimaging.

In our proof-of-principle experiment, the periodic domain structures of the PPLT crystal help create subwavelength foci with prescribed sizes and shapes, as the SH waves with different phases propagate freely and interfere destructively. The achievable subdiffraction patterns depend on parameters such as the periodicity of domain structures, sizes of the domain structures, and the propagation distance. Experimentally, superfocused SH spots with sizes of less than $\lambda_{\text{pump}}/8$ have been recorded at 27.5 μm away from the sample. In comparison with the superoscillatory experiment¹⁴ using a binary-amplitude metal mask, the current scheme explores the π phase difference between the SH fields generated from inside and outside of the domains, respectively. Note that such a π -phase shift does not exist in grating-based Talbot effect and linear superfocusing systems. Besides, the structure of the PPLT crystal does not involve complicated nano-fabrications and has large-scale parameters than light wavelengths.

Similar to our previous studies on SH Talbot effects^{24,25}, the super-focusing setup is schematically shown in Fig. 2. A femtosecond mode-locked Ti:sapphire laser was operated at a wavelength of $\lambda_{\text{pump}} = 900$ nm as the fundamental input field. The pulse width was about 75 fs with a repetition rate of 80 MHz. As illustrated in Fig. 2, the fundamental pump laser was first shaped by a pinhole and focusing lens to produce a near-parallel beam with a beam size of ~ 100 μm , and then directed into a 2D squarely-poled LiTaO₃ slice along the z axis with its polarization parallel to the x axis of the crystal. The sample with the size of 20 mm (x) \times 20 mm (y) \times 0.5 mm (z) was placed on a nanopositioning precision translation stage, and the SEM image of its domain structures (with a period of $a = 5.5$ μm and a duty cycle of $\sim 35\%$) is depicted in the inset of Fig. 2. Despite the LiTaO₃ crystal has a space group of $3m$ (C_{3v}), mainly the d_{21} component contributes to the SH generation in the current experimental configuration. After the sample, an objective lens ($\times 100$) with a high numerical aperture of $\text{NA} = 0.7$ was used to magnify the SH intensity patterns ($\lambda_{\text{SH}} = 450$ nm). With this secondary imaging process, the magnified SH intensity distributions were recorded by the CCD camera. To remove the near-infrared fundamental field, a bandpass filter was placed between the objective lens and the CCD camera. The SH patterns at different imaging

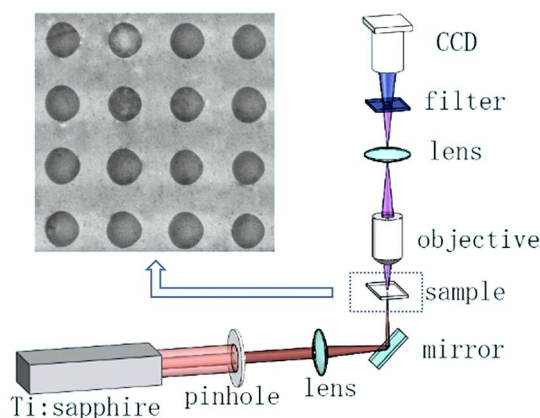


Figure 2 | Schematic diagram of the experimental setup. The sample is placed at the focal plane of the lens. The SH patterns at different imaging planes are recorded by a CCD camera mounted on a nanopositioning precision translation stage. Inset is the SEM image of the 2D squarely-poled LiTaO₃ slice with a period of 5.5 μm and duty cycle of $\sim 35\%$.



planes were recorded along the SH propagation direction by moving the microscope stage, which was controlled by the precision translation stage.

Experimental results. To ensure the good alignment requested in superfocusing, we begin with the observation of SH Talbot self-imaging in comparison with theoretical predictions. Characteristic SH field patterns recorded at different distances (Z) away from the output surface of the sample are presented in Fig. 3, representing a variety of “photonic carpets” in the Fresnel diffraction region. As indicated in Figs. 3a–f, the diffraction patterns change dramatically along with the focus being moved away from the crystal. The primary Talbot self-imaging was observed at $Z = 132.3 \mu\text{m}$ (Fig. 3f), which is well consistent with the theoretically calculated SH Talbot length^{24,25} of $Z_t = 4a^2/\lambda_{\text{pump}} = 134.4 \mu\text{m}$. One previously unconfirmed feature appears at about 1/2 Talbot length where a square array-like SH self-image is laterally shifted by half the width of the domain period (comparing Fig. 3c with Fig. 3f). In fractional Talbot planes, one can see complicated diffraction patterns, which result from the Fresnel diffraction interference of the SH waves. In proximity to the end face of the sample (Figs. 3a–d), the SH waves form periodic focused spots at the center of each unit. The focusing size varies with the propagation distance Z and superfocusing occurs at certain planes. At some other planes (e.g., 4/5 fractional Talbot plane as shown in Fig. 3e), the focusing spots disappear due to destructive interference. By carefully examining the patterns, one can find that the detailed structures in every single unit are very sensitive to the observation distance, especially when close to the sample. For example, as the observation plane moves from $Z = 3.5 \mu\text{m}$ (Fig. 3a) to $Z = 4.6 \mu\text{m}$ (Fig. 3b), the rings at the center shrink and the fractal array at the corner evolves. The key factor is that the phases of the SH waves develop sensitively along the propagation distance.

After confirming the alignment, we are ready to look for the subdiffracted SH spots at different propagation distances. According to the Abby resolution limit, the diffraction lower bound is about

321 nm in the current system. However, in the experiment we have recorded series of subwavelength focused spots at different propagation distances. Figure 4 shows some typical images with subdiffracted focused spots. For $\lambda_{\text{SH}} = 450 \text{ nm}$, at a distance of $Z = 27.5 \mu\text{m}$ a subdiffracted spot was identified with a full-width-at-the-half-maximum (FWHM) of 106 nm (see the enlarged area in Fig. 4a), i.e. $0.117 \times \lambda_{\text{pump}}$ or $0.235 \times \lambda_{\text{SH}}$, which surpasses that of the superoscillatory lens ($0.29 \times \lambda_{\text{pump}}$; a focal spot of 185 nm in diameter for a wavelength of 640 nm, Ref. 14). The recorded cross-section of the spot shown in Fig. 4e, without any data post-processing, is well fitted with a Lorentzian lineshape. The background is resulted from the imperfect domain structures. Due to the imperfections such as defects in the crystal and the nonuniform domain structures, not all the theoretically predicted superfocused spots were observable in the experiment. At $Z = 31.5 \mu\text{m}$ the selected subdiffraction spot (Fig. 4b) has a FWHM of 187 nm (Fig. 4f). We notice that in the current scheme, the cross-section profile of the measured subdiffracted spot fits better with a Lorentzian curve rather than with a Gaussian shape, which is in contrast to those focusing spots obeying the diffraction limit. For instance, at the distance of $Z = 91.4 \mu\text{m}$, a focusing spot with a size of 227 nm (close to the diffraction limit) is well fitted by a Gaussian curve (Figs. 4d and 4h). In the present experiment, the largest distance where we can still find superfocusing spots is at $Z = 133.4 \mu\text{m}$ (almost at the primary SH Talbot plane, Fig. 4c) and these subwavelength spots with a FWHM down to 168 nm (Fig. 4g) well follow a Lorentzian profile. We also carefully analyzed the power distribution in superfocusing. For the input pump power setting at 590 mW, the total power of the generated SH field is $\sim 4.64 \text{ mW}$. The power of each central superfocused spot in Fig. 4a–d is about (0.227, 1.236, 0.713, 1.269) nW, respectively. As expected, most of the energy is distributed in side fringes while the center spot contains less than one thousandth of the total SH power.

Simulations. To theoretically verify that the superfocusing feature in our experiment is indeed formed by the constructive/destructive interference of propagating SH waves, we performed numerical

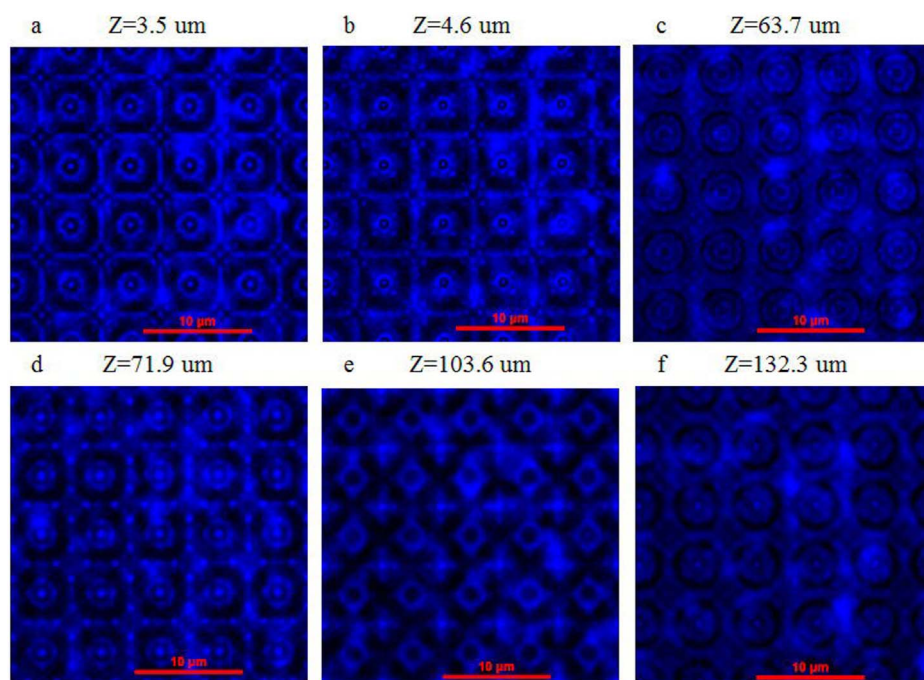


Figure 3 | Recorded images of the SH patterns with a conventional optical microscope at different Talbot planes. The images shown here are all formed within one Talbot length. (a) and (b) are close to the sample surface. (c) is the SH pattern at 1/2 Talbot plane, which is laterally shifted by half a period in comparison with the primary SH self-image, (f), at the first Talbot plane. Periodic focusing spots can be observed in most of the imaging planes. At certain planes (see (e)), however, the focusing spots disappear because of destructive interference of the SH waves.

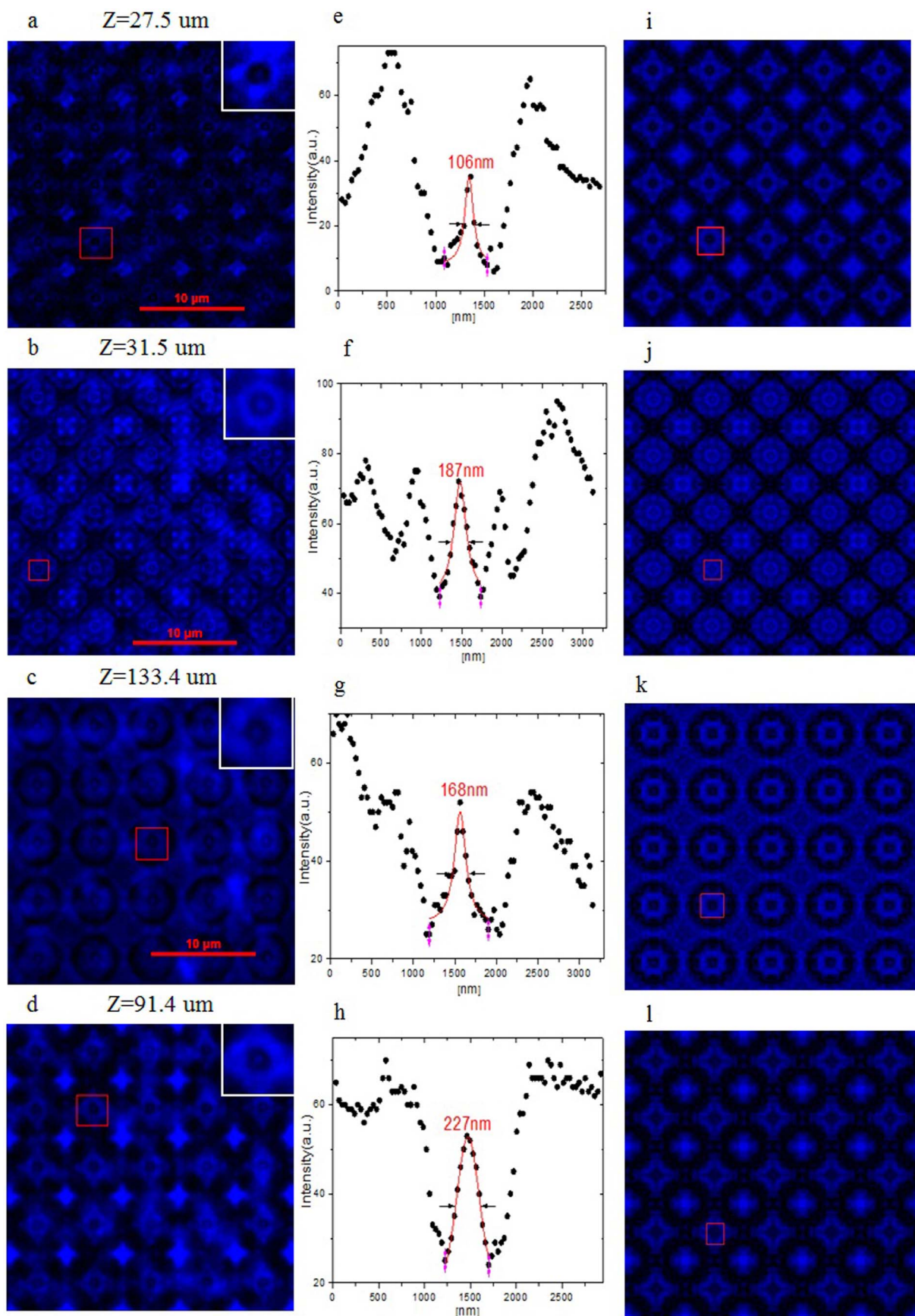


Figure 4 | Typical measured results of superfocusing. (a–d) are experimentally recorded SH patterns at different observation distances, where the insets are the enlarged images of the selected focused spots. The cross-sections of the selected focused spots in (a–d) are given, respectively, in (e–h), whose centers are fitted with a Lorentzian (e–g) or Gaussian (h) lineshape. The black dots in (e–h) are experimental data. (i–l) are theoretical simulations corresponding to (a) – (d), respectively.



simulations using the angular spectrum method. For the self-images shown in Figs. 4a–d, the simulations predict the same patterns as depicted in Figs. 4i–l by using the experimental parameters. For Figs. 4e–h, the simulations yield the focused spot sizes of 118 nm, 191 nm, 185 nm, and 225 nm, respectively, which indicate good agreements with the experimental data. Our simulations also reveal that the width of the domain walls is a very important parameter for the imaging pattern. We find, both theoretically and experimentally, that wide domain walls ($>1 \mu\text{m}$) may completely change the image patterns and eliminate the superfocusing phenomenon at those spatial planes. Thanks to the high-quality sample used in the experiment, the computed patterns by using a model without considering domain walls well match the experimental results. This implies that the domain walls here are narrow enough to be negligible in the process of image formations. To further examine the observed subdiffraction effect, we have chosen another hexagonally-poled PPLT structure with a period of $9 \mu\text{m}$ and the duty cycle $\sim 30\%$ (previously used for the illustration of SH Talbot effect^{24,25}). The input pump laser was still operated at the 900 nm wavelength. In the Fresnel near field, subwavelength focusing has also been observed (not shown here).

Discussion

One may notice that the CCD camera used in the experiment has pixels with the size of $6.45 \times 6.45 \mu\text{m}^2$. College textbook Optics tells us that a passive Gaussian thin lens won't lead to a subdiffracted focused spot for a plane-wave illumination. One interesting question then arises: how can one image the subwavelength spots from the focusing plane to the CCD camera? It turns out that in the spirit of superoscillations⁹, the superposed waves at the center superfocused spot can be *effectively* approximated as a new (pseudo-)wave with an *effective* wavenumber N times larger than the original SH wavenumber, where N is the resolution enhancement over the Abbe limit achieved in the experiment. The center focused spots with these effective wavenumbers therefore can be imaged in the CCD camera through the traditional imaging process as described above. Experimentally, we have further verified this analysis through looking at the size of a standard focused spot (following the Abbe diffraction limit, obtained after a Gaussian thin lens) magnified by passing another Gaussian lens. Different from this latter case, in our experiments we have observed different size amplification, which is a strong evidence of superoscillations. We notice that in the previous superoscillatory experiments^{13,14}, no such analysis has been implemented.

Subwavelength focusing with such a square array or hexagonal array PPLT could allow light to be squeezed into the scale of less than a quarter of the SH wavelength (i.e., less than one eighth of the fundamental wavelength!), thereby opening new avenues of studying light-matter interactions, single-molecule sensing, nanolithography, and nanoscale imaging. By optimizing the parameters (such as the periodicity, domain structure, and propagation distance), it is possible to shrink the focused spot size down to tens of nanometers, which would be comparable with those functional super-resolution imaging techniques^{20–23}. Moreover, thanks to the excellent electro-optic characteristics of PPLT, one may continuously tune the phase of the SH waves produced in the crystal, and control the interference and focusing in the far field by applying an electric field²⁸. To effectively remove the background noise, we have recently used concentrically poled nonlinear crystals^{26,27} by following the original proposal proposed by Toraldo di Francia⁷. The preliminary experimental results (not shown here) clearly show substantial improvement on the quality of the superfocused light spots.

Subdiffraction imaging holds many exciting promises in various areas of science and technologies. The extension of the current method to optical microscope may improve the resolving power down to nanometer scale, which would be very useful for non-invasive

subwavelength biomedical imaging. Another potential application is in optical lithography at ultra-small scales, which is the key to scaling down integrated circuits for high-performance optoelectronics. Optical data storage and biosensing may also benefit from this promising scheme to process information within an ultra-small volume, thereby increasing storage densities or sensing resolution.

In summary, we have proposed and demonstrated an easy way to reduce the point spread function below $\lambda_{\text{SH}}/4$ in SH Talbot effect with the periodically-poled LiTaO₃ crystal. The method does not involve evanescent waves nor subwavelength structures in the object. Through the destructive/constructive interference, the subdiffracted SH spots can be observed up to $133.4 \mu\text{m}$ away from the sample for $\lambda_{\text{pump}} = 900 \text{ nm}$. The numerical simulations have confirmed the experimental results with excellent agreements. Our work can be considered as the first realization of the proposals made by Toraldo di Francia⁷ and Berry & Popescu⁹. Furthermore, our investigation can potentially have a wide range of applications including subwavelength imaging, as a mask for biological molecule imaging, optical lithography and focus devices.

Methods

Model of the simulations. We used the same parameters of the sample to model the “aperture function”, and also took into account the π phase shift of the SH waves in negative domains. After propagation distance z , the diffracted SH field is computed by the Rayleigh–Sommerfeld diffraction formula²⁵:

$$U(x, y, z) = \int_{-f_m}^{f_m} \int_{-f_m}^{f_m} A_0(f_x, f_y) \exp[ikz \sqrt{1 - (\lambda f_x)^2 - (\lambda f_y)^2}] \exp[i2\pi(f_x x + f_y y)] df_x df_y,$$

where $A_0(f_x, f_y)$ is the angular-spectrum representation of the sample aperture function at $z = 0$. In the model, the SH field is simplified to be a plane wave, and the integration limits are bounded by the phase-matching condition in the range of $[-f_m, f_m]$. Despite this method allows accurate calculations on the evolution of intensity distribution recorded in the CCD camera, in light of weak measurement²⁹ superoscillations offer an alternative but interesting interpretation on the phenomenon.

1. Abbe, E. Beitrage zur theorie des mikroskops und der mikroskopischen wahrnehmung. *Arch. Mikrosk. Anat.* **9**, 413–468 (1873).
2. Serrels, K. A., Ramsay, E., Warburton, R. J. & Reid, D. T. Nanoscale optical microscopy in the vectorial focusing regime. *Nature Photon.* **2**, 311–314 (2008).
3. Kawata, S., Inouye, Y. & Verma, P. Plasmonics for near-field nano-imaging and superlensing. *Nature Photon.* **3**, 388–394 (2009).
4. Mosk, A. P., Lagendijk, A., Leroosey, G. & Fink, M. Controlling waves in space and time for imaging and focusing in complex media. *Nature Photon.* **6**, 283–292 (2012).
5. Oseen, C. W. Die Einsteinsche Nadelstichstrahlung und die Maxwellschen Gleichungen. *Ann. Phys. (Leipzig)* **374**, 202–204 (1922).
6. Schelkunoff, S. A. A Mathematical Theory of Linear Arrays. *Bell Syst. Tech. J.* **22**, 80–107 (1943).
7. Toraldo di Francia, G. Super-gain antennas and optical resolving power. *Suppl. Nuovo Cim.* **9**, 426–438 (1952).
8. Aharonov, Y., Anandan, J., Popescu, S. & Vaidman, L. Superpositions of time evolutions of a quantum system and a quantum time-translation machine. *Phys. Rev. Lett.* **64**, 2965–2968 (1990).
9. Berry, M. V. & Popescu, S. Evolution of quantum superoscillations and optical superresolution without evanescent waves. *J. Phys. A* **39**, 6965–6977 (2006).
10. Patorski, K. The self-imaging phenomenon and its applications. *Prog. Opt.* **27**, 1–108 (1989).
11. Wen, J.-M., Zhang, Y. & Xiao, M. The Talbot effect: Recent advances in classical optics, nonlinear optics, and quantum optics. *Adv. Opt. Photon.* **5**, 83–130 (2013).
12. Huang, F. M., Zheludev, N. I., Chen, Y. & Javier Garcia de Abajo, F. Focusing of light by a nanohole array. *Appl. Phys. Lett.* **90**, 091119 (2007).
13. Huang, F. M. & Zheludev, N. I. Super-resolution without evanescent waves. *Nano Lett.* **9**, 1249–1254 (2009).
14. Rogers, E. T. F. *et al.* A super-oscillatory lens optical microscope for subwavelength imaging. *Nature Mater.* **11**, 432–435 (2012).
15. Wen, J.-M., Du, S. & Xiao, M. Improving spatial resolution in quantum imaging beyond the Rayleigh diffraction limit using multiphoton W states. *Phys. Lett. A* **374**, 3908–3911 (2010).
16. Boto, A. N. *et al.* Quantum interferometric optical lithography: Exploring entanglement to beat the diffraction limit. *Phys. Rev. Lett.* **85**, 2733–2736 (2000).
17. Ambrose, E. J. A surface contact microscope for the study of cell movements. *Nature* **178**, 1194 (1956).
18. Pendry, J. B. Negative refraction makes a perfect lens. *Phys. Rev. Lett.* **85**, 3966–3969 (2000).



19. Zhang, X. & Liu, Z. Superlenses to overcome the diffraction limit. *Nature Mater.* **7**, 435–441 (2009).
20. Hell, S. W. Far-field optical nanoscopy. *Science* **316**, 1153–1158 (2007).
21. Gustafsson, M. G. Nonlinear structured-illumination microscopy: Wide-field fluorescence imaging with theoretically unlimited resolution. *Proc. Natl. Acad. Sci. U.S.A.* **102**, 13801–13806 (2005).
22. Rust, M., Bates, M. & Zhuang, X. Sub-diffraction-limit imaging by stochastic optical reconstruction microscopy (STORM). *Nature Methods* **3**, 793–796 (2006).
23. Dertinger, T. *et al.* Superresolution optical fluctuation imaging (SOFI). *Adv. Exp. Med. Biol.* **733**, 17–21 (2012).
24. Zhang, Y., Wen, J.-M., Zhu, S. N. & Xiao, M. Nonlinear Talbot effect. *Phys. Rev. Lett.* **104**, 183901 (2010).
25. Chen, Z.-H. *et al.* Fractional second-harmonic Talbot effect. *Opt. Lett.* **37**, 689–691 (2012).
26. Kasimov, D. *et al.* Annular symmetry nonlinear frequency converters. *Opt. Express* **14**, 9371–9376 (2006).
27. Saltiel, S. M. *et al.* Generation of second-harmonic conical waves via nonlinear Bragg diffraction. *Phys. Rev. Lett.* **100**, 103902 (2008).
28. Liu, D.-M., Zhang, Y., Chen, Z.-H., Wen, J.-M. & Xiao, M. Acoustic-optic tunable second-harmonic Talbot effect based on periodically-poled LiNbO₃ crystals. *J. Opt. Soc. Am. B* **29**, 3325–3329 (2012).
29. Aharonov, Y., Albert, D. Z. & Vaidman, L. How the result of a measurement of a component of the spin of a spin-1/2 particle can turn out to be 100. *Phys. Rev. Lett.* **60**, 1351–1354 (1988).

Acknowledgments

This work was supported by the National Basic Research Program of China (Nos. 2012CB921804 and 2011CBA00205), the National Science Foundation of China (Nos.

11274162, 61222503, 11274165 and 11021403), and the Science Foundation of Jiangsu Province (No. BK20140590), the New Century Excellent Talents in University, and the Priority Academic Program Development of Jiangsu Higher Education Institutions (PAPD).

Author contributions

The principle of superfocusing in nonlinear Talbot effect was suggested by J.W. and Y.Z. with contribution from M.X., D.L., D.W. and Z.C. performed the superfocusing experiments and data post-processing. X.H., G.Z. and S.N.Z. fabricated the 2D PPLT crystals. Optical characterization and modeling of the superfocusing were undertaken by D.L., D.W. and Z.C. under the guidance of Y.Z. and J.W. J.W., Y.Z. and M.X. supervised the project and wrote the manuscript with contributions from all co-authors. J.W., Y.Z., M.X., D.L., Z.C. and D.W. contributed to the discussions of results and planning of experiments.

Additional information

Competing financial interests: The authors declare no competing financial interests.

How to cite this article: Liu, D. *et al.* Diffraction Interference Induced Superfocusing in Nonlinear Talbot Effect. *Sci. Rep.* **4**, 6134; DOI:10.1038/srep06134 (2014).



This work is licensed under a Creative Commons Attribution-NonCommercial-ShareAlike 4.0 International License. The images or other third party material in this article are included in the article's Creative Commons license, unless indicated otherwise in the credit line; if the material is not included under the Creative Commons license, users will need to obtain permission from the license holder in order to reproduce the material. To view a copy of this license, visit <http://creativecommons.org/licenses/by-nc-sa/4.0/>